HYDROGEN NON-PREMIXED COMBUSTION IN ENCLOSURE WITH ONE VENT AND SUSTAINED RELEASE: NUMERICAL EXPERIMENTS

Molkov, V., Shentsov, V., Brennan, S., and Makarov, D.
Hydrogen Safety Engineering and Research Centre (HySAFER), University of Ulster, Shore Road, Newtownabbey, BT37 0QB, UK, v.molkov@ulster.ac.uk, shentsov-v@email.ulster.ac.uk, sl.brennan@ulster.ac.uk, dv.makarov@ulster.ac.uk

ABSTRACT

Numerical experiments are performed to understand different regimes of hydrogen non-premixed combustion in an enclosure with passive ventilation through one horizontal or vertical vent located at the top of a wall. The Reynolds averaged Navier-Stokes (RANS) computational fluid dynamics (CFD) model with a reduced chemical reaction mechanism is described in detail. The model is based on the renormalization group (RNG) k-ε turbulence model, the eddy dissipation concept (EDC) model for simulation of combustion, and the in-situ adaptive tabulation (ISAT) algorithm that accelerates the chemistry calculations by two to three orders of magnitude. The analysis of temperature and species (hydroxyl, hydrogen, oxygen, water) concentrations in time, as well as the velocity through the vent, shed a light on regimes and dynamics of indoor hydrogen fires. A well-ventilated fire is simulated in the enclosure at a lower release flow rate and complete combustion of hydrogen within the enclosure. Fire becomes under-ventilated at higher release flow rates with two different modes observed. The first mode is the external flame stabilised at the enclosure vent at moderate release rates, and the second mode is the self-extinction of combustion inside and outside the enclosure at higher rates. The simulations demonstrated a complex flow dynamics through the vent that leads to formation of the external flame or the self-extinction. The air intake into the enclosure at later stages of the process through the whole vent area is a characteristic feature of the self-extinction regime. This air intake is due to faster cooling of hot combustion products by sustained colder hydrogen leak compared to the generation of hot products by the ceasing chemical reactions inside the enclosure and hydrogen supply. In general, an increase of hydrogen sustained release flow rate will change fire regime from the well-ventilated combustion within the enclosure, through the external flame stabilised at the vent, and finally to the self-extinction of combustion throughout the domain.

KEYWORDS: Hydrogen safety, numerical experiment, CFD model, non-premixed combustion, well-ventilated fire, under-ventilated fire, external flame, self-extinction.

NOMENCLATURE

A_r	pre-exponent (consistent units)
a	speed of sound (m/s)
$C_{j,r}$	molar concentration of species j in reaction r (kmol/m^3)
c	specific heat (J/kg-K)
D	molecular diffusivity (m^2/s)
E	total energy (J/kg)
E_r	activation energy (J/kmol)
h	enthalpy (J/kg)
G_k	generation of kinetic energy due to mean velocity gradients (kg/ms-3)
G_b	generation of kinetic energy due to buoyancy (kg/ms-3)
g	gravity acceleration (m/s^2)
K_r	equilibrium constant for the reaction r (-)
k	turbulent kinetic energy (m^2/s^2); thermal conductivity (W/m/K)
$k_{f,r}$	forward rate constant for reaction r (consistent units)
$k_{b,r}$	backward rate constant for reaction r (consistent units)
M	Mach number (-)
N	number of chemical species in the system (-)
Pr	Prandtl number (-)
p	pressure (Pa)
R_m	source term (kg/m^3/s)
$R_{m,r}$	rate of species m production/ destruction in reaction r (consistent units)
Sc	Schmidt number (-)
S	source term (-)
S_m	entropy (-)
S_{ij}	rate-of-strain tensor (s^{-1})
T	temperature (K)

t time (s)
$u_{i,j,k}$ velocity components (m/s)
$x_{i,j,k}$ spatial coordinates (m)
Y mass fraction (-)

Greek

α inverse effective Prandtl number
β coefficient of expansion (-)
β_r temperature exponent (-)
Γ net effect of third bodies on the reaction rate
γ specific heat ratio (-)
$\gamma_{i,r}$ third-body efficiency of specie j in reaction r (-)
δ_{ij} Kronecker symbol
ε energy dissipation rate (m^2/s^3)
λ thermal conductivity (W/m/K)
μ dynamic viscosity (Pa s)
ν kinematic viscosity (m^2/s)
$\nu'_{m,r}$ stoichiometric coefficient for reactant m in reaction r (-)
$\nu''_{m,r}$ stoichiometric coefficient for product m in reaction r (-)
ξ length fraction of turbulent structures (-)
ρ density (kg/m^3)
τ time scale (s)
ω component of the flow velocity parallel to the gravitational vector (m/s)

Subscripts

atm atmospheric
E energy
eff effective
i,j,k spatial coordinate indexes
m index of chemical species
p pressure
t turbulent
r reaction index

Bars

$\bar{}$ Reynolds averaged parameters (-)
$\sim$ Favre averaged parameters (-)
$*$ fine scale quantities (-)
$\wedge$ Arrhenius reaction (-)

Constants and model parameters

$C_{1\varepsilon}$=1.42
$C_{2\varepsilon}$=1.68
$C_{3\varepsilon}= tanh|\omega/u|$
C_{μ}=0.0845
C_{ξ} volume fraction constant C_{ξ}=2.1277
C_{τ} time-scale constant C_{τ}=0.4082
R universal gas constant

1.0 INTRODUCTION

Unscheduled release of hydrogen followed by a jet fire in an enclosure with one vent is a possible incident/accident scenario with hydrogen and fuel cell system. Knowledge of hydrogen non-premixed flame behaviour in confined space is absent. There is no experimental data on this issue to authors' knowledge. Therefore a numerical study with use of a contemporary model is a way forward to understand underlying physical phenomena of indoor hydrogen fire. This study expands numerical experiments on under-ventilated hydrogen jet fire and self-extinction dynamics in an enclosure performed by authors recently [1] and exploits the same CFD model described in detail here. Large eddy simulation (LES) model with similar sub-models of turbulence, combustion, and more detailed reduced chemical reaction mechanism was applied recently for the simulation of spontaneous ignition of a sudden hydrogen release into a T-shaped mock-up pressure relief device [2].

The self-extinction of a hydrogen flame in an enclosure with one horizontal vent located at the top of one wall was reported for the first time in [1]. The analysis of the numerical experiment, especially of hydroxyl (OH) concentration, assisted in understanding of the self-extinction process. It was concluded that the use of averaged throughout the enclosure volume parameters during the under-ventilated fire can give an indication of the moment when combustion essentially reduces, however it can underestimate significantly the timing when the flame is fully ceased. The numerical experiments [1] demonstrated a complex pattern of flow through the vent in both directions during the under-ventilated fire. The complete self-extinction was observed when the whole vent area was occupied for a finite period of time by air intake into the enclosure. The reason of this observation was assumed to be the cooling of hot combustion products by the sustained hydrogen release and to some extent by heat transfer to the enclosure walls.

This study expands the initial numerical experiments performed in [1] and aims at understanding of indoor hydrogen fires in an enclosure with one horizontal or vertical vent located at the top of one wall and a sustained hydrogen release of constant flow rate and temperature. The study exploits the most

advanced modelling technique to get insights into different regimes of hydrogen jet fire indoors.

2.0 THE CFD MODEL DESCRIPTION

2.1 Governing equations of fluid dynamics

The governing equations are conservation of mass, momentum, energy and species respectively:

$$\frac{\partial \overline{\rho}}{\partial t} + \frac{\partial}{\partial x_j}(\overline{\rho}\widetilde{u}_j) = 0\,, \tag{1}$$

$$\frac{\partial \overline{\rho}\widetilde{u}_i}{\partial t} + \frac{\partial}{\partial x_j}(\overline{\rho}\widetilde{u}_j\widetilde{u}_i) = -\frac{\partial \overline{p}}{\partial x_i} + \frac{\partial}{\partial x_j}(\mu+\mu_t)\left(\frac{\partial \widetilde{u}_i}{\partial x_j} + \frac{\partial \widetilde{u}_j}{\partial x_i} - \frac{2}{3}\frac{\partial \widetilde{u}_k}{\partial x_k}\delta_{ij}\right) + \overline{\rho}g_i\,, \tag{2}$$

$$\begin{aligned}&\frac{\partial}{\partial t}(\overline{\rho}\widetilde{E}) + \frac{\partial}{\partial x_j}(\widetilde{u}_j(\overline{\rho}\widetilde{E}+\overline{p})) = \\ &= \frac{\partial}{\partial x_j}\left(\left(k + \frac{\mu_t c_p}{Pr_t}\right)\frac{\partial \widetilde{T}}{\partial x_j} - \sum_m \widetilde{h}_m\left(-\left(\rho D + \frac{\mu_t}{Sc_t}\right)\frac{\partial \widetilde{Y}_m}{\partial x_j}\right) + \widetilde{u}_i(\mu+\mu_t)\left(\frac{\partial \widetilde{u}_i}{\partial x_j} + \frac{\partial \widetilde{u}_j}{\partial x_i} - \frac{2}{3}\frac{\partial \widetilde{u}_k}{\partial x_k}\delta_{ij}\right)\right) + S_E\,,\end{aligned} \tag{3}$$

$$\frac{\partial \overline{\rho}\widetilde{Y}_m}{\partial t} + \frac{\partial}{\partial x_j}\left(\overline{\rho}\widetilde{u}_j\widetilde{Y}_m\right) = \frac{\partial}{\partial x_i}\left(\left(\rho D + \frac{\mu_t}{Sc_t}\right)\frac{\partial \widetilde{Y}_m}{\partial x_j}\right) + R_m\,. \tag{4}$$

2.2 Turbulence model

The renormalization group (RNG) *k*-*ε* turbulence model is applied that was derived from the instantaneous Navier-Stokes equations [3, 4]. The analytical derivation resulted in a model with constants different from those in the standard *k*-ε model, and additional terms and functions in the transport equations for *k* and ε. Transport equations for the turbulent kinetic energy, *k*, and the energy dissipation rate, ε, in the RNG *k*-ε turbulence model are:

$$\frac{\partial}{\partial t}(\rho k) + \frac{\partial}{\partial x_i}(\rho k u_i) = \frac{\partial}{\partial x_j}\left(\alpha_k \mu_{eff}\frac{\partial k}{\partial x_j}\right) + G_k + G_b - \rho\varepsilon - Y_M + S_k\,, \tag{5}$$

$$\frac{\partial}{\partial t}(\rho \varepsilon) + \frac{\partial}{\partial x_i}(\rho \varepsilon u_i) = \frac{\partial}{\partial x_j}\left(\alpha_\varepsilon \mu_{eff}\frac{\partial \varepsilon}{\partial x_j}\right) + C_{1\varepsilon}\frac{\varepsilon}{k}(G_k + C_{3\varepsilon}G_b) - C_{2\varepsilon}\rho\frac{\varepsilon^2}{k} - R_\varepsilon + S_\varepsilon\,, \tag{6}$$

where G_k represents the generation of turbulence kinetic energy due to the mean velocity gradients. Term G_k is evaluated in a manner consistent with the Boussinesq hypothesis as:

$$G_k = \mu_t S^2\,, \tag{7}$$

where S is the modulus of the mean rate-of-strain tensor S_{ij}, defined as $S = \sqrt{2S_{ij}S_{ij}}$. At the high Reynolds numbers the effective viscosity μ_{eff} is used instead of μ_t in Eq. 7, where $\mu_{eff} = \mu + \mu_t$, and the turbulent viscosity is calculated from the turbulence model:

$$\mu_t = \rho C_\mu k^2/\varepsilon\,, \tag{8}$$

where the constant C_μ=0.0845 instead of 0.0837 in the original work [3]. The generation of turbulence

kinetic energy due to buoyancy is equals to:

$$G_b = \beta g_i \frac{\mu_t}{Pr_t} \frac{\partial T}{\partial x_i}, \tag{9}$$

where Pr_t is the turbulent Prandtl number, $\beta = -(\partial\rho/\partial T)/\rho$ is the expansion coefficient, and g_i is the component of the gravitational vector in i-th direction. In the RNG k-ε model $Pr=1/\alpha_0$ with $\alpha_0=k/\mu c_p$, and $Pr_t=1/\alpha$, where α is calculated by the theoretical equation [3]:

$$\left|\frac{\alpha - 1.3929}{\alpha_0 - 1.3929}\right|^{0.6321} \left|\frac{\alpha + 2.3929}{\alpha_0 + 2.3929}\right|^{0.3679} = \frac{\mu}{\mu_t}. \tag{10}$$

For high Mach number flows, compressibility affects turbulence through so-called "dilatation dissipation", which is normally neglected in the modelling of incompressible flows [5]. Neglecting the dilatation dissipation fails to predict the observed decrease in spreading rate with increasing Mach number for compressible mixing and other free shear layers. To account for these effects in the k–ε models in ANSYS Fluent, the dilatation dissipation term, Y_M, is included in the k equation. This term is modelled according to Sarkar [6] as $Y_M = 2\rho\varepsilon M_t^2$, where $M_t = \sqrt{k/a^2}$ is a turbulent Mach number, and $a = \sqrt{\gamma RT}$ is the speed of sound.

The constants $C_{1\varepsilon}$=1.42, and $C_{2\varepsilon}$=1.68. The degree to which ε is affected by the buoyancy is determined by the constant $C_{3\varepsilon}$, which is calculated in ANSYS Fluent following [7] as $C_{3\varepsilon}=tanh|\omega/u|$, where ω is the component of the flow velocity parallel to the gravitational vector and u is the component of the flow velocity perpendicular to the gravitational vector. In this way, $C_{3\varepsilon}$ will become 1 for buoyant shear layers for which the main flow direction is aligned with the direction of gravity. For buoyant shear layers that are perpendicular to the gravitational vector, $C_{3\varepsilon}$ will become zero. The quantities α_k and α_ε in equations for k and ε respectively are the inverse effective Prandtl numbers for k and ε, respectively. The source terms S_k and S_ε are user-defined and equal to zero in this study.

The effective viscosity μ_{eff} is calculated using the RNG theory [3]. The RNG model is capable to reproduce not only turbulent, but also transitional and laminar flows. At low Reynolds numbers the effective viscosity becomes equal to molecular viscosity. This allows the model to perform better in the vicinity of walls [8]. The effective viscosity is calculated in RNG k-ε model of Fluent using a differential equation for turbulent viscosity:

$$d\left(\frac{\rho^2 k}{\sqrt{\varepsilon\mu}}\right) = 1.72 \frac{\hat{\nu}}{\sqrt{\hat{\nu}^3 - 1 + C_\nu}} d\hat{\nu}, \tag{11}$$

where $\hat{\nu} = \mu_{eff}/\mu$, and $C_\nu \approx 100$. This equation is integrated in Fluent to obtain an accurate description of how the effective turbulent transport varies with the effective Reynolds number (or eddy scale), allowing the model to better handle low Reynolds number and near-wall flows. In the limit of high Reynolds number Eq. 11 gives Eq. 8. The main difference between the RNG and standard k–ε model lies in the additional term in the ε equation given by (with $\eta=Sk/\varepsilon$, η_0=4.38, β=0.012):

$$R_\varepsilon = \frac{C_\mu \rho \eta^3 (1 - \eta/\eta_0)}{1 + \beta\eta^3} \frac{\varepsilon^2}{k}. \tag{12}$$

2.3 Combustion model

The eddy dissipation concept (EDC) model is an extension of the eddy dissipation model to include chemical reaction mechanism in a turbulent flow [9]. It assumes that reactions occur in small turbulent

structures, called the fine-scales. The length fraction of the fine-scales is modelled as [10]:

$$\xi^* = C_\xi \left(\frac{\nu \varepsilon}{k^2} \right)^{1/4}, \tag{13}$$

where * denotes to fine-scale quantities, C_ξ=2.1377 is the volume fraction constant and ν is the kinematic viscosity. Species are assumed to react in the fine structures over a time scale:

$$\tau^* = C_\tau \left(\frac{\nu}{\varepsilon} \right)^{1/2}, \tag{14}$$

where C_τ=0.4082 is a time-scale constant. In the EDC model the source term in the conservation equation for the mean species, Eq. 4, is modelled as [11]:

$$R_m = \frac{\rho (\xi^*)^2}{\tau^* \left[1 - (\xi^*)^3 \right]} (Y_m^* - Y_m), \tag{15}$$

where R_m is a net rate of production/destruction of species m by chemical reactions, ξ* is the length fraction of the fine-scale turbulent structures where the reaction occurs, Y_m^* is the fine-scale species m mass fraction after reacting over the time τ*, Y_m is a species mass fraction for species m in the surrounding fine-scales state [11]. The multiplier in above equation with a square of the length fraction of fine-scales represents the mass exchange between the surrounding and fine-structure regions.

Combustion at the fine-scales is assumed to occur as a constant pressure reactor, with initial conditions taken as the current species and temperature in the cell. Reactions proceed over the time scale τ*, governed by the Arrhenius rates (Eq. 16), and are integrated numerically using the in-situ adaptive tabulation (ISAT) algorithm by Pope [12] that can accelerate the chemistry calculations by two to three orders of magnitude, offering substantial reductions in run-times:

$$\hat{R}_{m,r} = \Gamma (\nu''_{m,r} - \nu'_{m,r}) \left(k_{f,r} \prod_{j=1}^{N} [C_{j,r}]^{\eta'_{j,r}} - k_{b,r} \prod_{j=1}^{N} [C_{j,r}]^{\eta''_{j,r}} \right), \tag{16}$$

where, $\hat{R}_{m,r}$ is the molar rate of creation/destruction of species m in reaction r, N is the number of chemical species in the system; $\nu'_{m,r}$ is the stoichiometric coefficient for reactant m in reaction r; $\nu''_{m,r}$ is the stoichiometric coefficient for product i in reaction r; $k_{f,r}$ and $k_{b,r}$ are forward and backward rate constants for reaction r respectively; $C_{j,r}$ is the molar concentration of species j in reaction r; $\eta'_{j,r}$ and $\eta''_{j,r}$ are rate exponent for reactant species j and product species j in reaction r respectively. Γ represents the net effect of third bodies on the reaction rate and is equal to $\Gamma = \sum_j^N \gamma_{j,r} C_j$, where $\gamma_{j,r}$ is the third body efficiency of j-th species in the r-th reaction. The forward rate constant for reaction r, $k_{f,r}$, is computed using the Arrhenius equation (see constants in Table 1):

$$k_{f,r} = A_r T^{\beta_r} e^{-E_r / RT}. \tag{17}$$

If the reaction is reversible, the backward rate constant for reaction r, $k_{b,r}$, is computed from the forward rate constant using the relation $k_{b,r} = k_{f,r} / K_r$, where K_r is the equilibrium constant for the r-th reaction, is computed from:

$$K_r = \left(\frac{p_{atm}}{RT} \right)^{\sum_{i=1}^{N} (\nu''_{m,r} - \nu'_{m,r})} \exp \left(\frac{\Delta S_r}{R} - \frac{\Delta H_r}{RT} \right), \tag{18}$$

where p_{atm} is the atmospheric pressure equal to 101325 Pa. The term within the exponential function represents the change in Gibbs free energy, and its components are computed as follows:

$$\frac{\Delta S_r}{R} = \sum_{m=1}^{N} (\nu''_{m,r} - \nu'_{m,r}) \frac{S_m}{R} \quad \text{and} \quad \frac{\Delta H_r}{RT} = \sum_{m=1}^{N} (\nu''_{m,r} - \nu'_{m,r}) \frac{h_m}{R}. \tag{19}$$

2.4 Chemical reaction mechanism

The 18-step reduced chemical reaction mechanism of hydrogen combustion in air is applied that is a subset of the Peters and Rogg's mechanism [13] that excludes H2O2 formation and consumption. Indeed, for the reactants at room temperature and not very large pressures up to 4 MPa, the H2O2 concentration is very low and does not play an important role in the structure of the flame [14]. The reduced mechanism counts eight reactive species (H2, O2, H, O, OH, HO2, H2O, N2). The effect of nitrogen chemistry is not taken into account and nitrogen plays a role of the third body only. The forward reaction rate constants are presented in Table 1, and backward rates for reversible reactions are calculated through the equilibrium constants, Eq. 18.

Table 1. Specific reaction rate constants [13].

No.	Reactions	A_r *	β_r	E_r, kJ/mol
H_2/O_2 Chain Reactions				
1	O2+H=OH+O	2.00E+14	0.00	70.30
2	OH+O=O2+H	1.568E+13	0.00	3.52
3	H2+O=OH+H	5.06E+04	2.67	26.30
4	OH+H=H2+O	2.222E+04	2.67	18.29
5	H2+OH=H2O+H	1.00E+08	1.60	13.80
6	H2O+H=H2+OH	4.312E+08	1.60	76.46
7	OH+OH=H2O+O	1.5E+09	1.14	0.42
8	H2O+O=OH+OH	1.473E+10	1.14	71.09
HO_2 Formation and Consumption				
9	O2+H+M=HO2+M	2.3E+18	0.80	0.00
	Third-body chaperon efficiencies H2O/6.5/ O2/0.4/ N2/0.4/			
10	HO2+M=O2+H+M	3.19E+18	-0.80	95.39
	Third-body chaperon efficiencies H2O/6.5/ O2/0.4/ N2/0.4/			
11	HO2+H=OH+OH	1.5E+14	0.00	4.20
12	HO2+H=H2+O2	2.5E+13	0.00	2.90
13	HO2+OH=H2O+O2	6.E+13	0.00	0.00
14	HO2+H=H2O+O	3.E+13	0.00	7.20
15	HO2+O=OH+O2	1.8E+13	0.00	-1.70
Recombination Reactions				
16	H+H+M=H2+M	1.8E+18	-1.00	0.00
	Third-body chaperon efficiencies H2O/6.5/ O2/0.4/ N2/0.4/			
17	OH+H+M=H2O+M	2.2E+22	-2.00	0.00
	Third-body chaperon efficiencies H2O/6.5/ O2/0.4/ N2/0.4/			
18	O+O+M=O2+M	2.9E+17	-1.00	0.00
	Third-body chaperon efficiencies H2O/6.5/ O2/0.4/ N2/0.4/			

* - the units for $\boldsymbol{A_r}$ are $[cm^3/(mol \times sec \times K^{\beta_r})]$ and $[cm^6/(mol^2 \times sec \times K^{\beta_r}]$ for bi-molecular and tri-molecular reactions respectively.

3.0 DETAILS OF NUMERICAL EXPERIMENTS

Numerical experiments were performed using ANSYS Fluent pressure-based solver with SIMPLE pressure-velocity coupling algorithm and spatial discretization of the first order, the gravity forces were applied.

3.1 Geometry, calculation domain and numerical grid

The enclosure was a cube with side size of 1 m characteristic for a fuel cell. There was only one vent in each simulation either horizontal or vertical. The vent was located at the top and at the central part of a wall. The release was directed vertically upward. Hydrogen release pipe was of 10 cm length with internal diameter of 5.08 mm located in the centre of the enclosure floor 10 cm above the floor. The thickness of the enclosure aluminium walls was 2 cm (each wall was resolved by 4 control volumes).

Two calculation domains were used and three grids created. Simulations with horizontal vent were carried out in a calculation domain in the form of a hexahedron of size *LxWxH*=7x6x4 m. Simulations with vertical vents were performed in a calculation domain of size *LxWxH*=5x2x4 m. Both domains included the enclosure and free space around. Seven numerical experiments were performed in total (Table 2).

The block-structured hexahedral grid was applied with finer mesh in areas of the release pipe and the enclosure vent. Tree different numerical grids were employed (one for each vent size). The total number of control volumes (CVs) in the domain of grid 1 with horizontal vent *HxW*=3x30 cm was 1,530,987 (the number of CVs in the enclosure was 229,746). The number of CVs along the vent height was 5, along the width – 33, along the depth – 4. There were 660 CVs inside the vent of grid 1. The total number of CVs in grid 2 with the vertical vent of size *HxW*=30x3 cm was 1,412,521 CVs (the number of CVs in the enclosure was 379,837). The number of CVs along the vent height was 30, along the width – 9, along the depth – 4. There were 1080 CVs inside the vent. The total number of CVs in grid 3 with vertical vent of size *HxW*=13.9x3 cm was 1,482,475 (there were 406,555 CVs in the enclosure). The number of CVs along the vent height was 24, along the – 9, along the depth – 4. There were 864 CVs inside the vent.

The hydrogen inflow boundary was a cross-section area of 45 CVs (9 CVs along the pipe diameter) located 5 cm from the pipe exit inside the pipe. The total number of CVs within the pipe was 450.

Table 2. Details of numerical experiments.

Experiment No. (grid)	Vent size, HxW	Release velocity, m/s	Flow rate, g/s	Numerical ignition, s	Result
No.1 (grid 1)	Horizontal 3x30 cm	600 m/s	1.0857	0.2-0.5	Self-extinction
No.2 (grid 1)	Horizontal 3x30 cm	300 m/s	0.5486	5.0-6.5	Self-extinction
No.3 (grid 1)	Horizontal 3x30 cm	150 m/s	0.2714	0.5-1.5	External flame
No.4 (grid 2)	Vertical 30x3 cm	600 m/s	1.0857	1.5-6.0	External flame
No.5 (grid 2)	Vertical 30x3 cm	60 m/s	0.1086	0.0-5.5	Well ventilated
No.6 (grid 3)	Vertical 13.9x3 cm	600 m/s	1.0857	0.0-6.0	Self-extinction
No.7 (grid 3)	Vertical 13.9x3 cm	300 m/s	0.5486	0.0-2.2	External flame

3.2 Initial and boundary conditions

Temperature of hydrogen released from the pipe was 273 K, and initial temperature of air in the domain was 293 K, i.e. 20 degree higher than temperature of leaking hydrogen. The release velocity was 60, 150, 300, or 600 m/s. The pipe was initially filled in with air. The composition of air in the simulations was taken as 20.7% by volume of oxygen and 79.3% of nitrogen. The sustained release of hydrogen was simulated, i.e. the mass flow rate and the temperature of hydrogen were both kept

constant. The initial pressure throughout the calculation domain was set to 101325 Pa. Domain outlet boundary conditions were set to the same pressure and temperature as in the calculation domain. Non-slip boundary condition was applied on all surfaces.

3.3 Numerical ignition

Numerical ignition of hydrogen-air mixture was realized by a patch with temperature 3000 K over the zone *LxWxH*=1x0.25x1 cm that comprises 62 CVs and touches the pipe exit on one side. The zone was chosen to include a region with near stoichiometric hydrogen-air mixture to facilitate the ignition. The ignition was initiated at the same time or shortly after the beginning of the release and kept until hydroxyl (OH) mole fraction would reach at least 0.01, which is generally accepted value associated with flame at normal conditions [10]. Time of ignition start and finish is given in Table 2.

4.0 RESULTS AND DISCUSSION

4.1 Well-ventilated fire

Figure 1 shows dynamics of well-ventilated hydrogen jet fire in numerical experiment No.5 (central cross-section area of the enclosure is shown) with lowest velocity of release of 60 m/s applied in this study. The vertical vent is located at the left wall. At the end of numerical experiment the fire is at quasi-steady state conditions. The reaction zone, which is associated with presence of hydroxyl radical OH, increases slightly in the period from 10 s to 65 s (Fig. 1, top left). There is practically no hydrogen leaving the enclosure (Fig. 1, top right). Mole fraction of hydrogen in the vent is negligible of the order of 2E-04. This indicates that the fire is well-ventilated in conditions of simulation No.5.

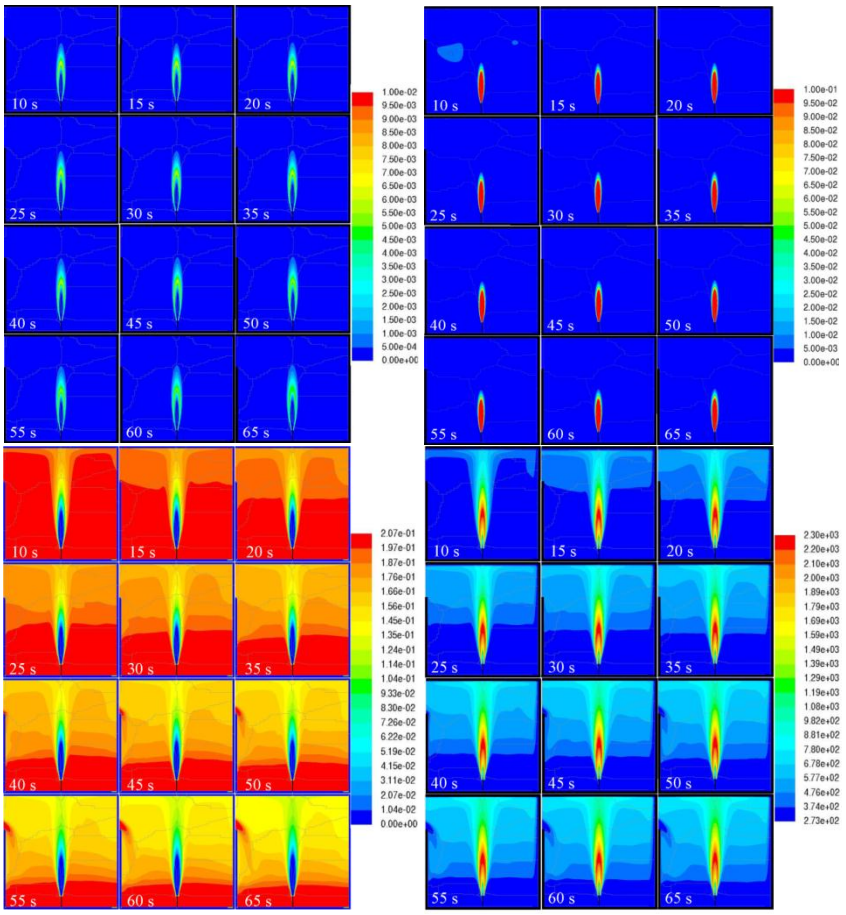

Figure 1. Mole fractions of OH (top left), H2 (top right), O2 (bottom left), and temperature (bottom right) in a 2D slice along the enclosure centre-line in simulation No.5 (well-ventilated fire)

Figure 1 (bottom left) shows that there is a very slow depletion of the initial oxygen layer at the bottom of the enclosure that can be explained by the fact that an intake of oxygen from outside the enclosure through the lower part of the vent to sustain the flame (the intake of air is clearly seen in snapshots). Temperature contours (Fig. 1, bottom right) confirm the presence of the layer at the bottom where the initial temperature is preserved. In room-like enclosure this would create favourable conditions for evacuation. It is worth noting that radiation is not accounted in this model that would affect acceptability of a safety engineering design based on harmful criteria of thermal radiation flux. Temperature decays from 2300 K in the flame to about 750-1000 K in the hot current under the ceiling. This temperature is probably insufficient to ignite any combustible materials especially in the presence of water vapour (H2O mole fraction under the ceiling is in the range 0.11-0.13 at 65 s). Yet some components within fuel cell box could be destroyed.

4.2 Transition to external flame

The only difference of numerical experiment No.4 considered in this section from simulation No.5 discussed in the previous section is tenfold increase of the hydrogen release flow rate. The well-ventilated fire is observed for hydrogen release velocity of 60 m/s, and an under-ventilated fire with transition to an external flame is observed for release velocity of 600 m/s.

Figure 2 demonstrates transition of an internal jet fire in the enclosure to an external flame. Mole fraction of hydroxyl in flame at 10 s is equal 0.01 that is characteristic for combustion at normal atmospheric conditions (not shown in Fig. 2). Then, maximum OH mole fraction reduces along with shrinking of the zone where highest mole fraction of OH is present. This is thought due to dilution of the jet flame by entrained combustion products. The maximum mole fraction of OH does not exceed 7.5E-03 at time 20 s. Figure 2 (top left) shows the evolution of the reaction zone during transition of the internal combustion to the external flame by visualization of OH mole fraction in the range1E-06÷5E-04, and Fig. 2 (top right) in the range 5E-04÷1E-03. There is no or little reaction outside the enclosure up to 20 s. While combustion rate inside the enclosure decreases after 20 s the reaction zone starts to move out of the enclosure through the vent with the external flame being seen above the enclosure after 50 s. Two top pictures in Fig. 2 clearly show that reaction ceases first on the jet flame side that is opposite to the vent which is located at the top of the left wall. Figure 2 (top left) demonstrates that there is a continuous reaction zone on both sides of the vent. This zone connects the internal reaction in the area where fresh air is entering the enclosure with the external flame of flowing out of the enclosure mixture of hydrogen and combustion products in atmospheric air. These two opposite direction flows through the vent create a reacting eddy that seats within the enclosure close to the vent and stabilises the lower flame edge. The upper edge of the external flame is attached to the top edge of the vent.

Evolution of H2 mole fraction in the enclosure is shown in Fig. 2 (middle left). Fire is in the well-ventilated regime until about 20 s when there is no hydrogen leaving the enclosure due to its complete combustion inside. The accumulation of hydrogen is somewhat higher at the side of the jet opposite to the wall with the vent. There is some inclination of the jet towards the vent (see snapshot 50 s). Mole fraction of hydrogen is above 0.30 practically throughout the whole enclosure at time 65 s with exclusion of small region close to the vent where air is entering. Mole fraction of H2 at 110 s is 0.48 to 0.50 at floor and ceiling level respectively.

The maximum amount of water vapour is observed at 27-30 s (Fig. 2 middle right), similar to simulation No.1 with horizontal vent of the same area reported in [1]. After this the mole fraction of water is monotonically decreases in time due to water entrainment into the sustained hydrogen jet and flow out of the enclosure (as a part of flammable mixture). At a critical point of flame "survival" at time about 50 s, when the transition to the external flame commences, the mole fraction of H2 in outflow increases to about 0.2, and of water (diluent) drops to 0.2-0.3. This mixture composition is deemed to be in the flammable range following the flammability diagram for hydrogen-air-diluent mixture at atmospheric pressure and temperature [14], if the effect of temperature is neglected. Thus,

the availability of flammable mixture flowing out of the enclosure and the presence of reaction (ignition source) provide conditions for transition of combustion outside of the enclosure.

Figure 2 (bottom left) shows that oxygen mole fraction within the enclosure gradually decreases and is practically equal to zero at 35 s excluding small area close to the vent. Then, air entering the enclosure to some small depth burns and is immediately entrained into flow of hydrogen and combustion products flowing out of the enclosure through the upper part of the vent. Temperature dynamics inside and outside the enclosure is shown in Fig. 2 (bottom right). The snapshot 50 s demonstrates an important role of the reacting eddy, which is formed in the vent shear layer between mixture leaving the enclosure and air entering the enclosure, on the flame sustainability and the transition of under-ventilated internal fire to the external flame mode.

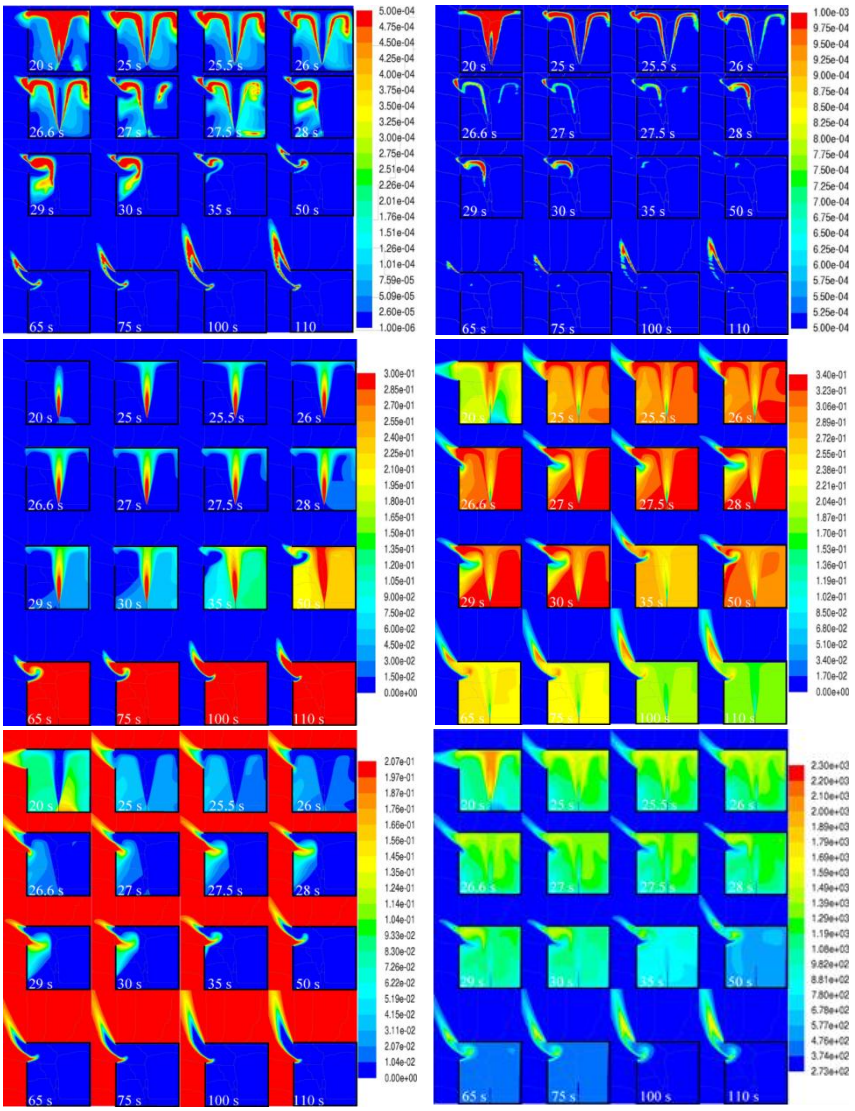

Figure 2. Mole fractions of OH in the range 1E-06÷5E-04 (top left) and OH in the range 5E-04÷1E-03 (top right), H2 (middle left), H2O (middle right), O2 (bottom left) and temperature (bottom right) in a 2D slice along the enclosure centre-line in simulation No.4 (external flame)

For the horizontal vent of the same area the establishment of external flame was observed in simulation No.3 at lower velocity of hydrogen exiting from the pipe of 150 m/s. The same velocity of release of 600 m/s (as in simulation No.4 with vertical vent) resulted for the horizontal vent in the flame self-extinction (simulation No.1, [1]). The self-extinction was observed also at velocity of 300

m/s (simulation No.2). Thus, a velocity limit separating the external flame mode and the self-extinction mode is between 150 m/s and 300 m/s for the horizontal vent.

External flame is observed in simulation No.7 with a vertical vent of smallest studied area and release velocity of 300 m/s. The increase of release velocity to 600 m/s (simulation No.6) resulted in the self-extinction. It is noted that a characteristic feature of the self-extinction phenomenon is the existence of a period when there is air intake into the enclosure through the whole area of the vent (not a part of the vent area).

4.3 Self-extinction of combustion throughout a domain

Self-extinction of hydrogen flame indoors was simulated and analysed for the first time in [1] for numerical experiment No.1 with the horizontal vent (see Table 2). It was found that there is a period of time from 27.5 s to 70 s when the whole vent area is occupied by flow of air into the enclosure. This is not the case for the transition to the external flame regime (see for example results of simulation No.4 discussed in previous section) when there is always a flow out of the enclosure, e.g. even through only 2 CVs as in simulation No.7 (external flame).

Let us now consider the dynamics of self-extinction observed in simulation No.2 with release velocity of 300 m/s and compare it with previous analysis of simulation No.1 (the release velocity of 600 m/s). Figure 3 shows the dynamics of OH mole fraction for simulation No.2 in 3D (left) and 2D (right). Reaction contour (OH mole fraction iso-surface of 1E-04) moves out of the enclosure at about 30 s. This zone of reaction outside the enclosure separates from the reaction zone inside the enclosure at 45 s and exists until about 56 s. The size of this external small reaction zone does not exceed two vent heights. At about the same time of 56-57 s there is air ingress into the enclosure that supports a weak reaction just below the vent. This internal reaction zone practically ceases at about 120 s. Contrary to experiment No.4 with the external flame, in simulation No.2 with the self-extinction, the combustion in the jet ceases first on the left side which is closer to the vent at 55-56 s. This can be explained and consistent with the presence of a bit larger amount of oxygen at this time at the bottom on the right hand side of the jet (see Fig. 4, bottom left).

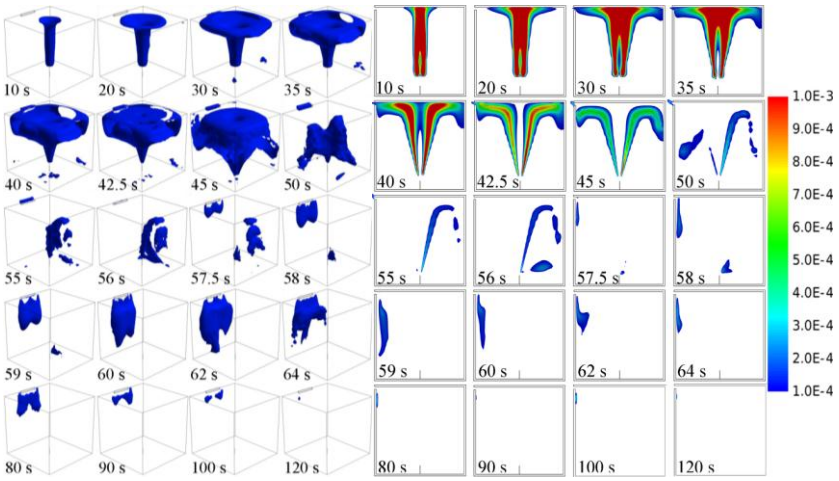

Figure 3. Mole fraction of hydroxyl OH in 3D (left, iso-surface of OH 1E-04), and 2D (right, a slice along the enclosure centre-line) in simulation No.2 (self-extinction)

The tiny size of the reaction zone outside of the enclosure in the period 30-56 s can be explained by analysis of species concentrations presented in Fig. 4. Indeed, during this period the concentration of hydrogen in flow out of the enclosure does not exceed about 7-10% by volume, concentration of water is increasing from about 15% to more than 34%, and oxygen concentration drops from about 10% to 0%. The flammability diagram shows that this mixture with air is just on the border of the flammable

region [14]. In simulation No.2 this mixture reacts with air in conditions that temperature of mixture is quite high and drops to about 800 K only at the end of this period.

The analysis of Fig. 4 demonstrates that the flow out of the enclosure finishes after 50 s and there is only inflow into the enclosure is seen in snapshots 57.5 s through to 120 s. Thus, in the agreement with simulation No.1 for the self-extinction to happen there has to be a prolonged period of time when, after the initial stage of internal combustion followed by the cooling of hot products by "cold" hydrogen, there is an intake of air through the whole area of the vent into the enclosure.

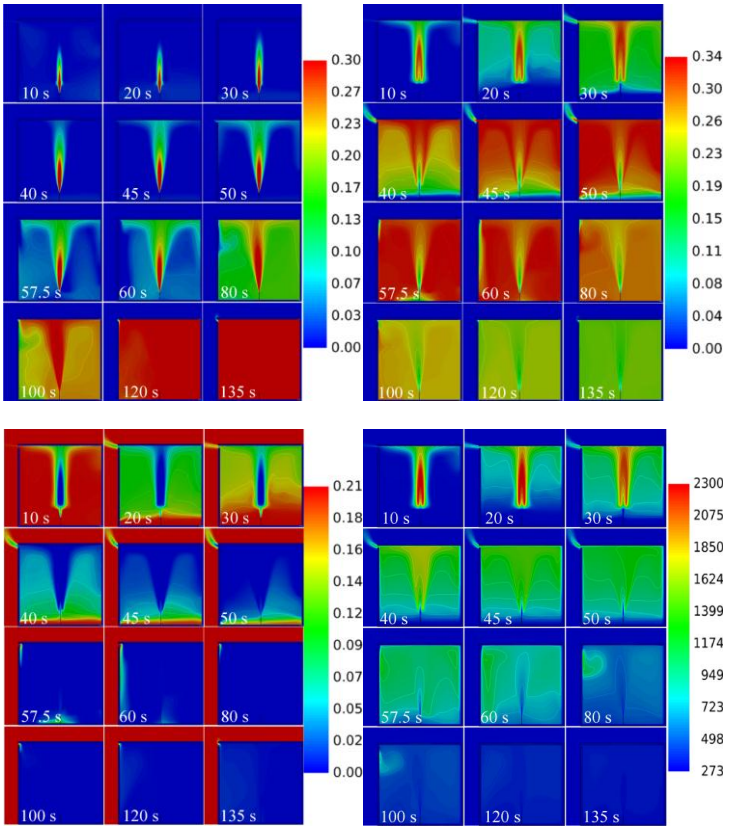

Figure 4. Mole fractions of H2 (top left), H2O (top right), and O2 (bottom left), and temperature (bottom right) in a 2D slice along the enclosure centre-line in simulation No.2 (self-extinction)

Figure 4 (top left) shows that after two minutes of the release the enclosure is filled in with hydrogen with mole fraction above stoichiometric 0.30. Similar to simulation No.4 with vertical vent the jet is slightly inclined to the wall with the vent. The maximum mole fraction of water is observed at 50-60 s. There is strong "stratification" of oxygen at time 40-50 s with practically zero concentration at the top and practically initial concentration of oxygen of 20.7% by volume at the bottom. Temperature falls down to about 100 degree above initial temperature after two minutes of ignited release. This result can be used as an indication of fire resistance time to components within the enclosure (fuel cell).

The former conclusion that the self-extinction is always observed when there is a period of time when there is air intake into the enclosure through the whole vent area is confirmed in experiment No.6 with the vertical vent of lowest area. To further support this rule of thumb, in simulations No.7 (external flame) there was no such period (while there was tiny outflow out of the enclosure through only two CVs at the top corners of the vent).

There is a flame lift-off seen in Fig. 4. In this particular simulation (No.2) the numerical ignition patch was elevated with respect to the pipe exit (in all other numerical experiments the patch was "touching" the pipe). Figure 3 (right) shows that the lift-off distance decreases with time. Another potential reason for this lift-off could be infinitely thin wall of the pipe in simulations.

4.4 Effect of release flow rate on combustion time inside the enclosure

Figure 5 shows maximum volumetric fraction of hydroxyl radical OH within the enclosure as a function of time in numerical experiments No.1-3 with the horizontal vent. The initial peak of OH mole fraction is associated with a manual procedure of numerical ignition and high temperature of the patch of 3000 K that is above the adiabatic flame temperature. In simulation No.2 with release velocity of 300 m/s the numerical ignition was delayed by 5 s. The mole fraction of OH is stabilised after the numerical ignition at level of about 0.01 for all three simulations.

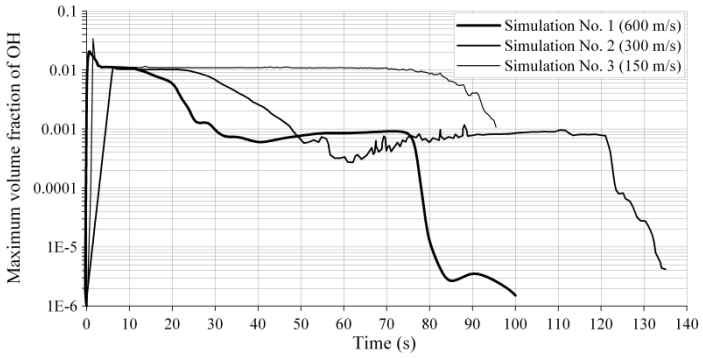

Figure 5. The dynamics of maximum hydroxyl (OH) volume fraction within the enclosure in simulations No.1-3

The initial stage of combustion in the enclosure is similar to a free jet flame in the open atmosphere as the depletion of oxygen and the dispersion of combustion products in the enclosure and their entrainment into the hydrogen jet can be neglected. However, after a period of time the maximum mole fraction of hydroxyl OH starts to reduce monotonically to a small value, which can be sustained quite for a while, before OH concentration drops to zero (reaction inside the enclosure ceases). The higher the release flow rate the shorter the period of "well-ventilated" fire when sufficient amount of oxygen is available within the enclosure before transition to the external flame (simulation No.3) or self-extinction (simulations No.1-2).

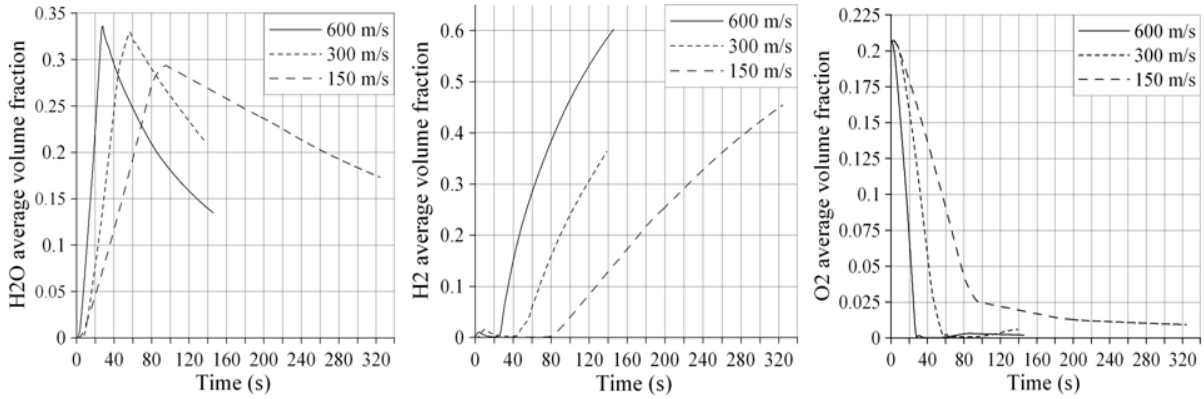

Figure 6. Averaged volumetric fraction of species in the enclosure as a function of time: water (left), hydrogen (centre), oxygen (right) in simulations No.1-3

Figure 6 shows volumetric fractions of water (H2O), hydrogen (H2), and oxygen (O2), which are averaged through the enclosure volume, as a function of time. The maximum of H2O mole fraction in the enclosure is at time 27.5 s, 58 s and 95 s for tests No.1-3 respectively. These times coincide with time when the average hydrogen concentration starts to increase as its consumption due to combustion is practically stopped (Fig. 6, centre), and oxygen concentration is decreased significantly and cannot sustain initial combustion rate (Fig. 6, right). The conclusions about flame self-extinction based on the

average values of species in the enclosure should be done with care. Indeed, there are small areas in the enclosure where reactions continue. These small reaction areas are located close to the vent.

4.3 Pressure effect of indoor jet fire

Figure 7 shows averaged through the enclosure overpressure, generated by hydrogen jet fire in simulations No.1-4,7 (from left to right respectively), as a function of time. The maximum overpressure drops for the same horizontal vent from 300 Pa for release velocity 600 m/s to 75 Pa for 300 m/s and to about 25 Pa for 150 m/s. The rule of thumb for simulations with the horizontal vent is that the decrease of flow rate by two will result in the reduction of overpressure generated by the indoor fire by 3-4 times. It is worth noting that these overpressures are far below the lower limit for damage to low strength equipment and civil structures of 10 kPa. The vertical vent of the same area is less effective for reduction of the indoor jet fire overpressure than horizontal vent (both located at the top of the wall). This is due to the known fact that venting of gases of smaller density is more efficient for pressure reduction. Indeed, the overpressure in simulation No.4 with vertical vent is about 365 Pa, i.e. 65 Pa higher compared to simulation No.1 with horizontal vent of the same area.

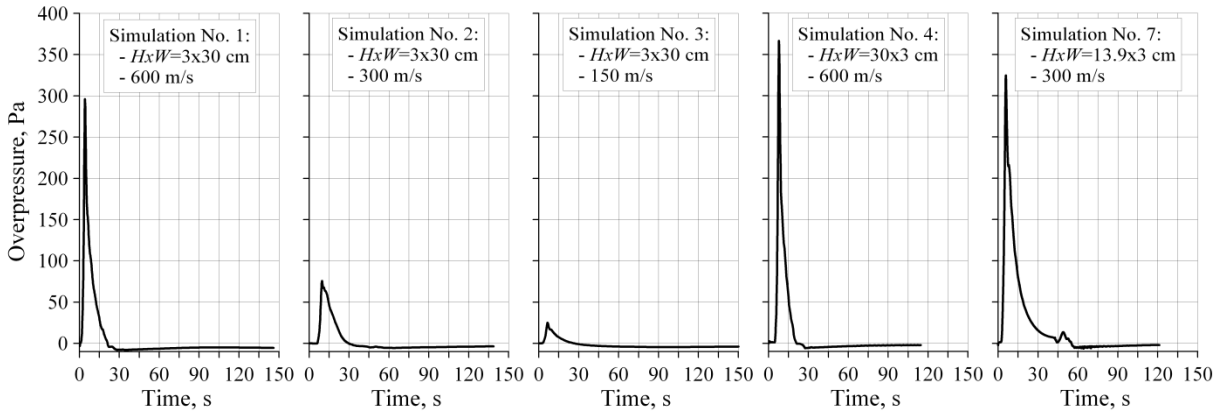

Figure 7. Averaged overpressure (relative to the operating pressure) within the enclosure as a function of time in simulations No.1-4,7 (from left to right respectively)

In all simulations after the pressure peak generated by intensive combustion of hydrogen within the enclosure the average overpressure becomes negative at time of about 22 s for experiment No.1, 30 s for No.2, 27 s for No.3, and 21.3 s for No.4, 55 s for No.7. Then average overpressure remains negative until the end of simulations due to cooling of hot gases inside the enclosure by continuous release of hydrogen with temperature 20 degrees below the ambient and heat transfer to the walls.

There is a period of pressure oscillations after fast pressure drop in all simulations. Duration of this period is different and often associated with flame flickering. For example, sustained oscillations with amplitude of about 0.1-0.2 Pa are observed in simulation No.4 after 60 s up to the end of simulations at 115 s, and stronger oscillations with amplitude up to 1.3 Pa in period 57-70 s (then oscillations amplitude decreases) with oscillation period of about 1.3 s for simulation No.7.

5.0 CONCLUSIONS

Seven numerical experiments are performed to simulate hydrogen non-premixed combustion in an enclosure of size 1x1x1 m with passive ventilation through one horizontal vent *HxW*=3x30 cm (release velocities 600, 300, 150 m/s), or one vertical vent of size *HxW*=30x3 cm (600 and 60 m/s) or *HxW*=13.9x3 cm (600 and 300 m/s). The contemporary CFD model is applied to simulate combustion dynamics with chemical reactions. The small release rate (velocity of 60 m/s) resulted in the well-ventilated regime of hydrogen fire in the enclosure with the vertical vent *HxW*=30x3 cm (hydrogen completely burned within the enclosure). The tenfold increase of hydrogen release velocity to 600 m/s has led to formation of the external flame stabilised at the enclosure vent while jet flame inside the

enclosure ceased. The decrease of the vertical vent size to *HxW*=13.9x3 cm at the same velocity 600 m/s led to the complete self-extinction of combustion in the whole domain. The increase of release velocity from 150 m/s to 300-600 m/s has led to the change of combustion regime from the external flame to the self-extinction respectively. It is concluded that as a general rule the increase of hydrogen flow rate changes fire regime in the enclosure from the well-ventilated fire, through transition of internal combustion to the external flame at moderate flow rates, and to the complete self-extinction of combustion at higher flow rates. Thus, two modes of under-ventilated fire are observed in this study. One mode is the external flame, and another is the self-extinction of flame. The model is planned to be used as a contemporary tool for hydrogen safety engineering after its validation against experiments planned for 2013-2014 within the HyIndoor project (www.hyindoor.eu).

6.0 ACKNOWLEDGEMENTS

The authors express their gratitude to the Fuel Cells and Hydrogen Joint Undertaking for funding this research through the HyIndoor project (grant agreement No. 278534).

7.0 REFERENCES

1. Molkov, V., Shentsov, V., Brennan, S., Makarov, D., "Dynamics of Hydrogen Flame Self-Extinction in a Vented Enclosure," *Proceedings of the 7th International Seminar on Fire and Explosion Hazards"*, 5-10 May 2013, Providence, RI, USA.
2. Bragin, M.V., Makarov, D.V., Molkov, V.V., "Pressure limit of hydrogen spontaneous ignition in a T-shaped channel," International Journal of Hydrogen Energy, (2013), accepted for publication.
3. Yakhot, V., Orszag, S., "Renormalization group analysis of turbulence. I. Basic theory." Journal of Scientific Computing, 1:3-51 (1986).
4. Orszag, S.A., Yakhot, V., Flannery, W.S., Boysan, F., Choudhury, D., Maruzewski, J., Patel, B., "Renormalization Group Modeling and Turbulence Simulations". In International Conference on Near-Wall Turbulent Flows, Tempe, Arizona. 1993.
5. Wilcox, D.C., Turbulence Modeling for CFD. DCW Industries, Inc. La Canada, California. 1998.
6. Sarkar, S., Balakrishnan, L., "Application of a Reynolds-Stress Turbulence Model to the Compressible Shear Layer". ICASE Report 90-18NASA CR 182002. 1990.
7. Henkes, R.A.W.M., van der Flugt, F.F., Hoogendoorn, C.J., "Natural Convection Flow in a Square Cavity Calculated with Low-Reynolds-Number Turbulence Models". Int. J. Heat Mass Transfer, 34: 1543–1557 (1991).
8. Shah, R.K., Heikal, M.R., Thonon, B., Tochnon, P., "Progress in the numerical analysis of compact heat exchanger surfaces." In: Hartnett, J.P. (Ed.) Advances in Heat Transfer, 34, 2001, San Diego, USA, Academic Press.
9. Magnussen, B.F., "On the structure of turbulence and a generalized eddy dissipation concept for chemical reactions in turbulent flow." *Proceedings of the 19th American Institute for Aeronautics and Astronautics Aerospace Science Meeting*, 12-15 January 1981, St. Louis.
10. Gran, I.R., Magnussen, B.F., "A numerical study of a bluff-body stabilized diffusion flame. Part 2. Influence of combustion modeling and finite-rate chemistry", *Combustion Science and Technology*, 119: 191 (1996).
11. Magnussen, B.F., "Modelling of pollutant formation in gas turbine combustors based on the eddy dissipation concept," *Proceedings of the CIMAC Conference*, 4-9 June, 1989, Tianjin, China.
12. Pope, S.B., "Computationally efficient implementation of combustion chemistry using in-situ adaptive tabulation", *Combustion Theory and Modeling*, 1: 41–63 (1997).
13. Peters, N., Rogg, B., Reduced Kinetic Mechanisms for Applications in Combustion Systems. *Lecture Notes in Physics*, Volume m15. Springer-Verlag, 1992.
14. Trevino, C., Mauss, F., Chapter 10 "Structure and Extinction of Non-Diluted Hydrogen-Air Diffusion Flames", In: Peters, N., Rogg, B., Reduced Kinetic Mechanisms for Applications in Combustion Systems. *Lecture Notes in Physics*, Volume m15. Springer-Verlag, 1992.
15. NASA Safety Standard for Hydrogen and Hydrogen Systems. Guidelines for hydrogen system design, materials selection, operations, storage, and transportation. Technical Report NSS

1740.16, Office of Safety and Mission Assurance, Washington, 1997. Available from: http://www.hq.nasa.gov/office/codeq/doctree/canceled/871916.pdf. NSS 1740.16 was cancelled on July 25 2005. [Accessed 05.04.13].